AFRL-AFOSR-JP-TR-2019-0037

Wearable biosensing platforms using 2D native protein fibers

Young Kim
PURDUE UNIVERSITY
401 SOUTH GRANT ST
WEST LAFAYETTE, IN 47907-2024

07/29/2019
Final Report

Air Force Research Laboratory
Air Force Office of Scientific Research
Asian Office of Aerospace Research and Development
Unit 45002, APO AP 96338-5002

REPORT DOCUMENTATION PAGE

Form Approved
OMB No. 0704-0188

1. REPORT DATE *(DD-MM-YYYY)*	2. REPORT TYPE	3. DATES COVERED *(From - To)*
29-07-2019	Final	27 Sep 2016 to 26 Sep 2017

4. TITLE AND SUBTITLE
Wearable biosensing platforms using 2D native protein fibers

5a. CONTRACT NUMBER

5b. GRANT NUMBER
FA2386-16-1-4114

5c. PROGRAM ELEMENT NUMBER
61102F

6. AUTHOR(S)
Young Kim, Kyung Min Byun

5d. PROJECT NUMBER

5e. TASK NUMBER

5f. WORK UNIT NUMBER

7. PERFORMING ORGANIZATION NAME(S) AND ADDRESS(ES)
PURDUE UNIVERSITY
401 SOUTH GRANT ST
WEST LAFAYETTE, IN 47907-2024 US

8. PERFORMING ORGANIZATION REPORT NUMBER

9. SPONSORING/MONITORING AGENCY NAME(S) AND ADDRESS(ES)
AOARD
UNIT 45002
APO AP 96338-5002

10. SPONSOR/MONITOR'S ACRONYM(S)
AFRL/AFOSR IOA

11. SPONSOR/MONITOR'S REPORT NUMBER(S)
AFRL-AFOSR-JP-TR-2019-0037

12. DISTRIBUTION/AVAILABILITY STATEMENT
A DISTRIBUTION UNLIMITED: PB Public Release

13. SUPPLEMENTARY NOTES

14. ABSTRACT
By capitalizing on natural nanomaterials/nanostructures, our research is focused interactions of light with some of native protein fibers found in nature. In search of biogenic nanomaterials/nanostructures for strong light scattering, native silk appears to be an ideal candidate. Specifically, 'silvery' and 'lustrous' appearance native silk, produced by Bombyx mori or Araneae, gives us a clue for taking advantage of irregular nanostructures, while possibly scaling up to flexible or wearable devices. The unique nanoarchitecture inside silk fibers can allow for strong light localization and efficient nanomaterial hybridizations. Our main founding can be summarized as 'silk is a natural metamaterial, which is an oxymoron', because strong light scattering (light localization in the Anderson regime) is a property not found in nature; it might bring up a new understanding of white 'blackbody'. First, we have found that the combination of native silk and facile metal nanoparticle hybridization offers not only nontoxic media, but also utilizes plasmonics. This idea is inspired by a common method in the 19th century of adding metal to the thread to increase the weight of silk fabrics and raise the sale price. The unprecedentedly strong affinity of silk to metal ions, which we initially intended to use as a biosensing mechanism, forms nanoparticulated metal with finite sizes inside silk. The combination of enhanced light-matter interactions and preferable binding features of silk could further be used to monitor specific physiological and biological changes in the body. In addition, the hybridization of mNPs into the fibrillar nanostructures of silk can offer plasmon-sensitized photocatalysis using visible light (or solar illumination). Fluorescent silk can also serve as light-induced electron donors and photoinducible radical-generating nanomaterials, which can inactivate harm

15. SUBJECT TERMS
speckle;, biosensing;, silk

16. SECURITY CLASSIFICATION OF:			17. LIMITATION OF ABSTRACT	18. NUMBER OF PAGES	19a. NAME OF RESPONSIBLE PERSON
a. REPORT	b. ABSTRACT	c. THIS PAGE			KNOPP, JEREMY
Unclassified	Unclassified	Unclassified	SAR		19b. TELEPHONE NUMBER *(Include area code)* 315-227-7006

Standard Form 298 (Rev. 8/98)
Prescribed by ANSI Std. Z39.18

Wearable biosensing platforms using 2D native protein fibers (FA2386-16-1-4114)
Final Performance Report
PI: Young L. Kim (Purdue University), youngkim@purdue.edu

By capitalizing on natural nanomaterials/nanostructures, our research is focused on interactions of light with some of native protein fibers found in nature. Recent experiments have revealed that light waves can undergo strong light scattering in the same manner of Nobel Prize winner Philip Anderson's theory. This possibility has the potential for a variety of biomedical applications, including biosensing. However, typical natural materials are intrinsically limited for strong light scattering as light is freely diffusing in such media. 'Silvery' and 'lustrous' appearance resulting from strong light scattering of native silk, produced by *Bombyx mori* or *Araneae*, gives us a clue for taking advantage of irregular nanostructures, while possibly scaling up to flexible or wearable devices and producing large quantities in an eco-friendly manner. In search of biogenic nanomaterials/nanostructures for strong light scattering, native silk appears to be an ideal candidate. Native silk is quasi-2D optical nanostructures, as illustrated in Fig. 0. This nanoarchitecture of silk can allow for unprecedentedly strong light-matter interactions and efficient nanomaterial hybridizations.

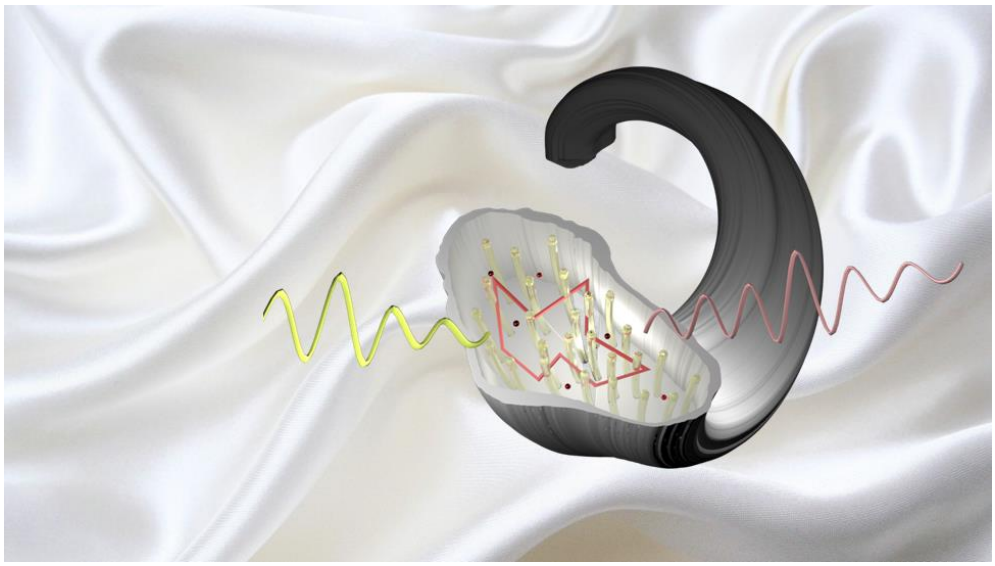

Fig. 0: Schematic illustration of light interactions with numerous nanofibrils in a native silk fiber.

Chapter 1: We have found that the unique combination of native silk and facile metal nanoparticle hybridization offers not only nontoxic media, but also utilizes plasmonics. This idea was inspired by a common method in the 19th century of adding metal salt to the thread to increase the weight of silk fabrics and raise the sale price. The unprecedentedly strong affinity of silk to metal ions, which we initially intended to use as a biosensing mechanism, forms nanoparticulated metal with finite sizes inside silk. Specifically, the combination of enhanced light-matter interactions and preferable binding features of silk could potentially be used to monitor specific physiological and biological changes in the body. In addition, the hybridization of mNPs into the fibrillar nanostructures of silk can offer plasmon-sensitized photocatalysis using visible light (or solar illumination). Fluorescent silk can also serve as light-induced electron donors and photoinducible reactive oxygen radical-generating nanomaterials, which could potentially be used to inactivate harmful pathogens.

Chapter 2: While studying the biochemical composition of native silk, we have realized that the protein and amino acid structures of native silk give rise to the strong absorption in the infrared region (IR) where solar radiation is negligible and thermal radiation is dominant. By Kirchhoff's identity, the high absorption leads to a high thermal emissivity in IR. Through the thermal radiation property of the biochemical compositions of native silk, strong light scattering in silk gains a functionality that controls radiation heat transfer. Taking advantage of mesoscopic physics theory, we have found one hidden mechanism in nature (passive radiative cooling), which can protect the pupa against an excessive external radiative heat source. Native silk possesses two distinct thermal and photonics mechanisms. The brilliant whiteness of silk, resulting from strong light localization in the Anderson regime, mostly reflects sunlight in the visible and NIR range. Owing to the polymeric characteristics, silk enhance the emissivity in the IR range where solar radiation is negligible and thermal radiation is dominant.

Our finding can be summarized as "silk is a natural metamaterial: an oxymoron", because Anderson light localization is a property not found in nature; it might bring up a new understanding of white 'blackbody'. Based on the known biocompatibility and bioresorbability of silk, these novel functionalities can further be combined with biosensing platforms for prolonged monitoring of physiological and biological changes. Our results provide the groundwork as a nanomaterial hybridization platform to implement embedded functionalities in a fiber geometry, which can easily be constructed into large-area fabrics. The superior optical and thermal properties of native silk could potentially be a building block for large-area flexible photonics and for a scalable hybridization platform of multifunctional nanomaterials. We also envision that our findings could potentially lead to a novel class of artificially engineered bionic materials in a variety of defense applications.

Chapter 1: Scalable/continuous nanomaterial hybridization of native and fluorescent silk

Abstract

For widespread practical translation and utilization of plasmonics and nanophotonics, there is always a need for scalable, cost-effective, eco-friendly, and nontoxic production of nanomaterials and nanostructures. As alternative fabrication and synthesis approaches, insects have received considerable attention as bioreactors and biosynthesis factories. However, scalable fabrication of plasmonic nanomaterials and their integration into flexible and wearable components are still limited. We show that a unique combination of silkworm factory and green chemistry appears to be an effective hybridizing platform for integrating natural biomaterials and metal nanoparticles. Our approach is inspired by a two-century-long method of increasing the weight of silk fabrics for high price (also known as silk weighting). The reported plasmonics hybridization of silk results in formation of silver nanoparticles in the interfibrillar space of silk fibers, which is manifested by the 'lustrous' or 'silvery' color of silk. We further demonstrate that plasmon-enhanced photoluminescence of far-red fluorescent protein in silk produced by genetically engineered silkworms (i.e. silkworm transgenesis). Our results provide the groundwork for exploiting native silk as a photonic hybridization platform to implement embedded functionalities in a fiber geometry, which could easily be woven or constructed into large-area and continuous fabrics using existing textile infrastructures in a sustainable manner.

Introduction

Plasmonic nanomaterials and nanostructures are extensively utilized in a variety of biomedical, energy harvesting, and photonics applications. Several studies have also been reported on their integration into wearable and implantable devices. From a nanofabrication and nanomanufacturing standpoint, it is critical to produce photonic nanomaterials and nanostructures and to further assemble them into higher-order components and systems in a scalable, economical, eco-friendly, and sustainable manner. In particular, it is highly beneficial to realize two crucial features: i) large-area and continuous nanomaterials and nanostructures with functional fabrics[1,2] (e.g. biosensing, communication, and hazard protection) and ii) eco-friendly and nontoxic production on an industrially relevant scale. Indeed, the actual manufacturing processes of current most energy-efficient nanodevices often consume large amounts of fossil fuel and raw materials, resulting in negative environmental consequences[3]. In this respect, there is always a combined need for both flexible/scalable/biosafe functionalities and green manufacturing/production for plasmonic nanomaterials and nanostructures for the widespread practical translation and utilization.

Among other insects (e.g. earthworms[4]), silkworms have received considered attention as bioreactors and insect factories for producing recombinant proteins, biomaterials, and hybrid nanomaterials.[5-11] Polymeric materials from silk proteins (i.e. fibroin) are often processed and fabricated into a variety of types of materials and structures, including optical components (e.g. lenses, prisms, diffraction gratings, and waveguides)[12-14]. While the engineering approaches (i.e. silk protein processing) are highly promising, the direct use of native silk fibers, which are produced via biological processing of silk proteins (i.e. fiber spinning from silkworms or spiders)[15-17], has their own advantage as a hybridization platform of nanomaterials and nanostructures. Specifically, we can take use of existing textile technologies and infrastructures

that may allow us to manufacture high-quality plasmonic nanoproducts in a large quantity and an affordable cost.

Toward this direction in conjunction with plasmonics, we take advantage of a unique silk property, inspired by a common practice in the 19th century for increasing the weight of silk fabrics. After degumming silk (i.e. removing the outer sericin layer to improve the color, sheen, and texture of silk), the weight loss can easily be compensated by soaking silk fabrics in a bath of metal salts (e.g. tin, iron, and lead)[18-20]. Silkworm silk fibers contain numerous amino acids, including tyrosine residues that have strong electron donating complex properties.[16,21,22] Based on this binding property, we propose to form nanoparticulated silver inside silk fibers to allow coupling of the electrons of silver nanoparticles (AgNPs) and electromagnetic waves. For plasmonic investigations, finite sized AgNPs are crucial for generating coupled electromagnetic-electron waves. Metal or inorganic nanoparticles are often integrated with silk fibers and fabrics for antibacterial activities and unique colorations[23-30]. However, our approach is distinct from such nanomaterial hybridizations and chemical functionalizations with silk, which are focused on coating or attaching metal nanoparticles (mNPs) on the surface of silk fibers. Another advantage of nanoparticulated Ag inside silk fibers is that AgNPs with finite sizes may not exhibit direct toxicity, while Ag ions released from AgNPs are known to be harmful[31]. Thus, wholly integrated AgNP-silk complexes could potentially reinforce plasmonic effects for full integration of natural proteins and synthetic nanomaterials into large-area and continuous substrates or clothes.

We show that native silk produced by silkworms (*Bombyx mori*) appears to be an alternative platform for hybridizing natural biomaterials and mNPs via simple green chemistry. Using the unprecedentedly strong affinity of silk proteins to metal ions, nanoparticulated silver with finite sizes are formed in the interfibrillar space of silk fibers, resulting in the 'lustrous' or 'silvery' color of silk. For plasmon-enhanced light-matter interactions, we use fluorescent protein-expressing silk, produced by transgenic silkworms[5,6,8], for selective excitation and emission originating from localized surface plasmon resonances of AgNPs inside silk fibers. Specifically, we demonstrate strong emission enhancement of mKate2 fluorescent protein in AgNP-embedded silk. Our results provide the groundwork for exploiting native silk as a photonic nanomaterial hybridization platform for implementing embedded functionalities in a fiber geometry, which can easily be woven or constructed into fabrics using conventional textile infrastructures. We further anticipate our biogenic hybridization route to be a starting point for possibly scaling up flexible and wearable photonic components in an eco-friendly, scalable, and sustainable manner.

Results and Discussion

We realize all-in-one plasmonic silk composed of AgNP-embedded native and transgenic silk fibers. The hybridization of finite sized AgNPs into silk is based on three unique features: the internal nanostructures of silk fibers, the strong binding property to metal ions, and facile green chemistry. First, we actively utilize the fibrillar nanostructures of silk fibers as a physical frame for hybridization. A natural silk fiber (~ 20 – 50 μm in diameter) consists of twin fibroin filaments and each filament is assembled from a bundle of highly packed nanofibrils (~ 20 – 200

nm)[20,32-35]. Indeed, the unique gland environment of silkworms and fibroin chemistry promote crystallization of nanofibrils with void interfibrillar space.[15-17] Second, exploiting the strong binding property to metal ions, we effectively infiltrate Ag metal salts into the nanofibrillar structures of natural silk. Third, we further enhance this hybridization process, using tannic acid (TA) ($C_{76}H_{52}O_{46}$, a plant derived polyphenolic compound) as an eco-friendly reducing and stabilizing agent for synthesizing AgNPs[36,37]. As historically used for burns treatments and as an alkaloid reagent[38,39], our TA concentration is minimized to reduce potential adverse effects (e.g. protein denaturation). We note that low concentrations of TA have been generally employed in dyeing and printing silk fabrics[40]. Specifically, we generate AgNP-embedded silk fibers using facile synthesis processes in aqueous solutions with only three basic chemicals of TA, $AgNO_3$, and K_2CO_3 at room temperature. For a systematic synthesis, we prepare for AgNP-embedded silk with different densities of AgNPs by controlling the mole ratio of $AgNO_3$ and the treatment time.

For nanostructural characterizations, we focus on using an optical means for characterizations. Due to polymeric nature of silk proteins (e.g. low atomic weight, low density protein, and rapid degradation under an electron beam), it is challenging to visualize the composite of AgNPs and silk using conventional electron microscopy[20,32,33]. Thus, we intensively use RCM to directly visualize the spatial distribution of AgNPs inside silk fibers, which exhibit slightly bright brown silk cocoons compared to the pure white color of native silk cocoons (Fig. 1a). It is virtually impossible to determine the exact sizes of AgNPs using RCM, due to a limited spatial resolution of RCM. On the other hand, RCM is highly beneficial for 3D visualization of AgNPs, because plasmonic resonances enhance the scattering cross sections of mNPs. For example, the scattering cross section of an AgNP with a diameter of 59 nm at λ = 488 nm is 8.1 times larger than the geometrical cross section. In Fig. 1b-d, bright spots inside silk fibers are easily seen on the same optically sectioned plane inside the fiber for three different laser illumination wavelengths of λ = 488, 543, and 633 nm. This representative visualization is performed from silk embedded with a low density of AgNPs by dissolving a small amount of $AgNO_3$ (i.e. 0.5 mM) with a short treatment time of five minutes. Fig. 1b-d show that AgNPs inside silk are formed relatively uniformly across the single imaging plane. The accumulated number of embedded AgNPs is significantly larger than that attached on the surface (Fig. 1e and video in ESI†). The spatial distributions of bright spots in Fig. 1b-d are not identical, because different laser wavelengths are sensitive to different plasmonic resonance bands that correspond to different dominant sizes of AgNPs. To further confirm the interfibrillar existence of AgNPs, we examine both inside and surface of AgNP-embedded silk fibers using EDX and SEM (Fig. 1f). From EDX of AgNP-embedded silk fibers, Ag is detected with 0.58 ± 0.15 (mean ± standard deviation) in weight percent (wt. %) inside silk fibers and 0.7 ± 0.15 wt. % on the surface (Fig. 1g). We also observe randomly distributed AgNPs inside silk fibers from TEM.

For AgNP-embedded silk, we can control the density and size of AgNPs formed in the interfibrillar space of silk by adjusting a mole ratio of $AgNO_3$ and a treatment time (Fig. 2e). In Fig. 2a and 2b, the optical extinction (or absorption) spectra are attributable to the superposition of plasmon resonances from individual AgNPs. As the mole ratio of $AgNO_3$ or the treatment time increase, the extinction peaks of AgNP-embedded silk become stronger and broader, because both density and size of AgNPs in silk are augmented. The maximum absorption peak position of AgNP-embedded silks at around

470 nm is relatively invariable (Fig. 2a and 2b). On the other hand, aqueous AgNP solutions, synthesized without the interfibrillar frame (without silk fibers), result in broader absorption spectra at larger mole ratios. For photoluminescent utilizations, a high density of AgNPs is not desirable, due to reabsorption of emission (also known as the inner filter effect). In general, mNPs have high extinction coefficients larger than conventional fluorophores[41]. Thus, we select a relatively low-density AgNP-embedded silk (mole ratio of $AgNO_3$ = 0.5 mM and treatment time = 5 minutes) that has 32.5% light absorption compared to native bare (control) silk (Table S1). Using Mie theory[42,43], we further estimate a size distribution of AgNPs inside silk fibers (Fig. 2c and 2d), assuming uniform spherical shapes of AgNPs, the known complex refractive index of Ag[44], and the refractive index of silk (~ 1.56[45]). To inversely estimate the size distribution of AgNPs, we use a lognormal distribution, which a solution-based AgNP synthesis typically follows[46], for the probability p as a function of the particle diameter d with two parameters μ and σ:

$$p(d) = \frac{1}{d\sigma\sqrt{2\pi}} \exp\left[-\frac{(\ln d - \mu)^2}{2\sigma^2} \right], \quad (1)$$

where $\log(p)$ is distributed normally with a mean of μ and a standard deviation of σ. This theoretical analysis suggests that a mode diameter of AgNPs in silk is 36 nm with μ = 3 and σ = 0.34. This result is in relatively good agreement with AgNPs in TEM. Importantly, we note that this AgNP hybridization with silk can further be extended to large-area or continuous fabrics with flexibility and wearability (Fig. 3). The integration of AgNPs into silk leads to no considerable variations in the mechanical properties of individual fibers. The mechanical properties of individual silk fibers, including the maximum strain, the maximum stress, and the Young's modulus, are not significantly changed after the AgNP hybridization with silk. In other words, the conventional textile methods can be used as scalable processes for further integration into higher-order manmade structures of fabrics.

To further embody innocuous nontoxic fluorophores in silk for plasmon-enhanced photoluminescence, silkworm transgenesis is an attractive route for producing wholly natural fluorescent silk fibers. By means of a popular germline transformation (i.e. *piggyBac* transposon)[5,6,8], we use genetically engineered domesticated silkworms (*Bombyx mori* bivoltine strain) to express monomeric far-red fluorescent protein (mKate2) in silk filaments. The transformation vector p3xP3-EGFP-pFibH-mKate2 is constructed as the *piggyBac*-derived vector and the vector DNA is injected with a helper vector into pre-blastoderm embryos. The analyses using high-performance liquid chromatography with tandem mass spectrometry confirm the expression of FibH chain-mKate2 fusion proteins. In transgenic silk, the mass density of mKate2/Fibroin H-chain fusion recombinant protein is estimated to be ~ 12.6 %. The produced mKate2 silk cocoon has a reddish color under white light illumination, resulting from its absorption and emission bands. Considering the spectral characteristics of plasmon resonances of AgNPs (0.5 mM and 5 minutes in Fig. 2) and mKate2 absorption/emission, it appears that AgNP-embedded mKate2 silk is an excellent photoluminescent platform, assisted by excitation enhancement of a stronger electric field or emission enhancement from a plasmon-coupled state[47-51].

To characterize plasmon-enhanced photoluminescence in AgNP-embedded mKate2 silk (Fig. 4a), we collectively excite AgNP plasmon resonances that mostly overlap with the absorption

band of mKate2. In Fig. 4b, the fluorescent confocal and RCM images on the same optically sectioned plane indicate colocalization of mKate2 and AgNPs in silk, respectively. In Fig. 4c, the excitation enhancement from the increased electric field in the vicinity of AgNPs gives rise to the stronger emission intensity in a mesoscopic (between microscopic and macroscopic) imaging setup (excitation band λ_{ex} = 470 – 550 nm and emission band λ_{em} = 600 – 700 nm). The photoluminescence spectra (Fig. 4d) clearly reveal that an enhancement ratio of AgNP-embedded mKate2 silk relative to bare mKate2 silk is 2.1 in the emission wavelengths of 600 – 700 nm. To estimate an average separation distance between mKate2 and AgNPs, we also model the enhancement ratio (E) of the fluorescent intensity, using the single-molecule fluorescence model[47-50].

$$E = \frac{\gamma_{ex}}{\gamma_{ex}^{0}}(\lambda_{ex})\frac{q}{q^{0}}(\lambda_{em}), \qquad (2)$$

where λ_{ex} is the excitation rate, λ^0_{ex} is the corresponding excitation rate in free space, q is the quantum yield of spontaneous emission coupled into the plasmon resonance, q^0 is the corresponding quantum yield in free space (≈ 0.4 for mKate2), λ_{ex} is the excitation wavelength, and λ_{em} is the emission wavelength of mKate2. In the excitation rate, we also incorporate the size distribution of AgNPs (Fig. 2d) obtained from the Mie calculations. An average separation distance between mKate2 and AgNPs weighted by their size distribution is likely to be ~ 30 nm (Fig. 4e) with the low density of AgNPs. Importantly, we can rule out a possibility that the mKate2 emission enhancement is attributed simply from changes in the scattering strength, resulting from the presence of AgNPs in silk. As shown in the reflectance images in two wavelength ranges of 470 – 550 nm (corresponding to λ_{ex}) and 600 – 700 nm (λ_{em}), both bare mKate2 silk and AgNP-embedded mKate2 silk are nearly indistinguishable, while the average reflectance value of AgNP-embedded mKate2 silk is slightly lower (i.e. ~ 5%) than that of bare mKate2 silk at λ_{ex} = 470 – 550 nm, due to the absorption of AgNPs (Fig. 2a and 2b). The mKate2 silk with higher AgNP densities shows decreased emission intensity, possibly due to reabsorption of AgNPs and quenching of mKate2. Thus, the reported results support the idea that AgNP-embedded silk is a scalable plasmonics route for minimal reabsorption of mNPs and plasmon-enhanced photoluminescence.

Conclusions

Exploiting native silk, green chemistry-based AgNP formation, and fluorescent proteins from silkworm transgenesis, we have demonstrated that the presented nanomaterial and nanostructure hybridization can serve as an affordable and scalable platform to realize plasmonics with large-area and flexible characteristics. Inspired by the two-century-long practice of increasing the weight for higher price of silk, AgNP-embedded fluorescent silk can provide immediately exploitable photonic nanomaterial and nanostructural hybridizations potentially for photocatalysis, energy harvesting, and biomedical applications. Specifically, the hybridization of mNPs into the fibrillar nanostructures of silk can offer plasmon-sensitized photocatalysis using visible light (or solar illumination)[52,53]. The fluorescent protein-expressing silk fibers can also have phototoxic effects upon light stimulation, because fluorescent proteins can serve as light-induced electron donors and photoinducible genetically-encoded reactive oxygen species-generating proteins[54,55]. These potential functionalities are ideal combinations with the strong light scattering of silk, which is manifested by the color of silk. Fluorescent

proteins and silk materials are also well-known for biocompatibility (or biodegradability) and high mechanical strength (e.g. stiffness and toughness). Thus, all of the superior properties associated with plasmonic silk will provide a building block for developing future multifunctional smart textiles. We also envision that the silkworm insect factory could potentially open an alternative green manufacturing strategy for producing plasmonic nanomaterials and nanostructures for integrated systems in an eco-friendly, scalable, and sustainable manner, minimizing the use of sophisticated nanofabrication methods.

Acknowledgements
This work was supported by Cooperative Research Program for Agriculture Science & Technology Development (PJ011835) from Rural Development Administration, South Korea and Asian Office of Aerospace Research and Development (FA2386-16-1-4114) from Air Force Office of Scientific Research, USA.

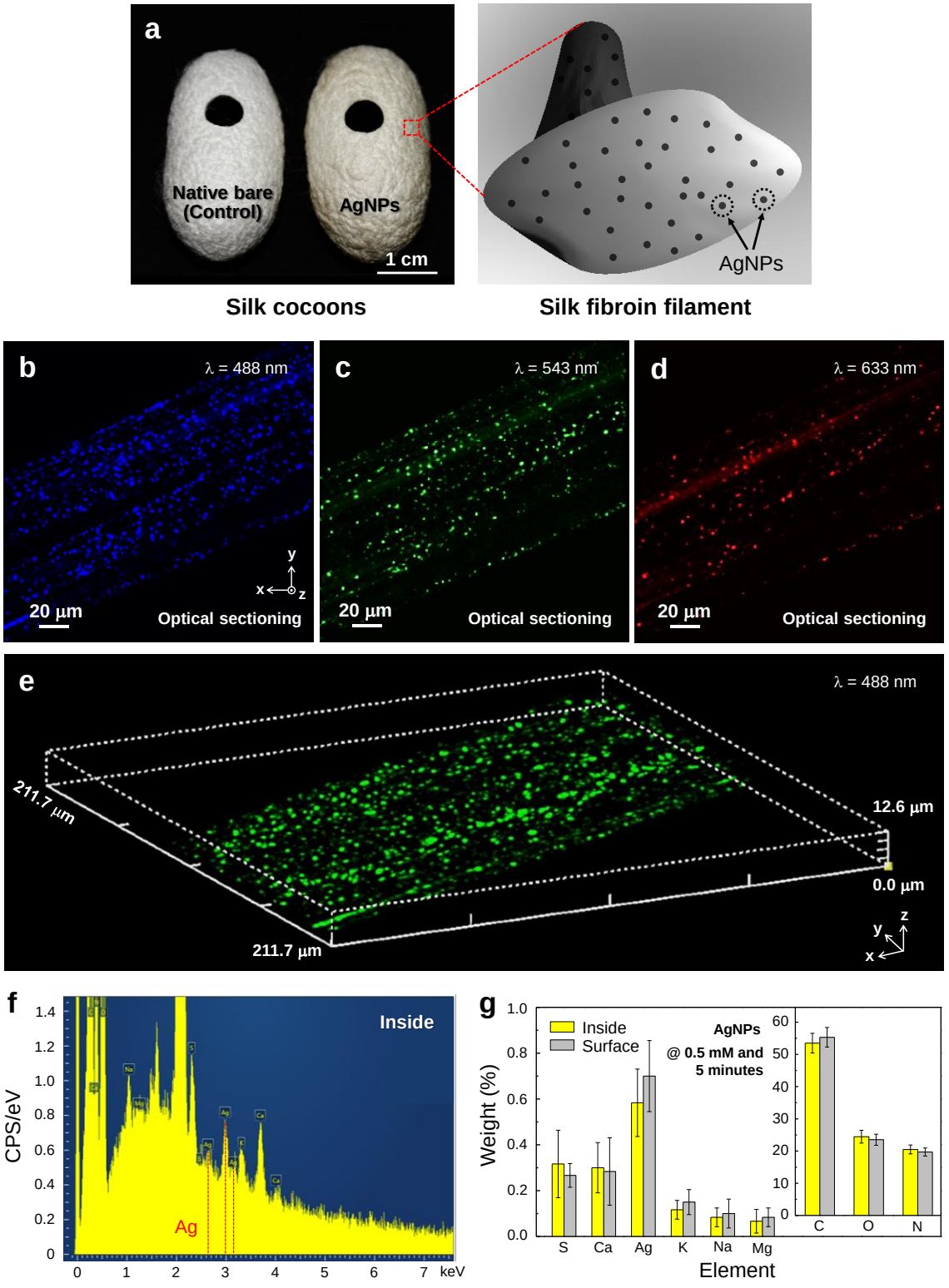

Fig. 1: Cooperative hybridization of AgNPs with native (*Bombyx mori*) silk. (a) Photographs of bare native (control) and AgNP-embedded silk cocoons with punched holes. Schematic illustration of AgNP-embedded silk filaments. (b-d) 2D optical sections and (e) 3D stack of

reflectance confocal microscopy (RCM) images of AgNP-embedded silk fibers under different laser illuminations at λ = 488 nm, 543 nm, and 633 nm. (f&g) Energy dispersive X-ray (EDX) spectrum (inside) and element data from AgNP-embedded silk fibers with a low density of AgNPs (i.e. mole ratio of $AgNO_3$ = 0.5 mM and treatment time = 5 minutes), which is an optimal condition for photoluminescence. EDX results show that silk contains the main three elements of carbon (C), nitrogen (N), and oxygen (O), including other minor elements of sulfur (S), calcium (Ca), potassium (K), sodium (Na), and magnesium (Mg). Importantly, native bare silk fibers do not show any element of Ag.

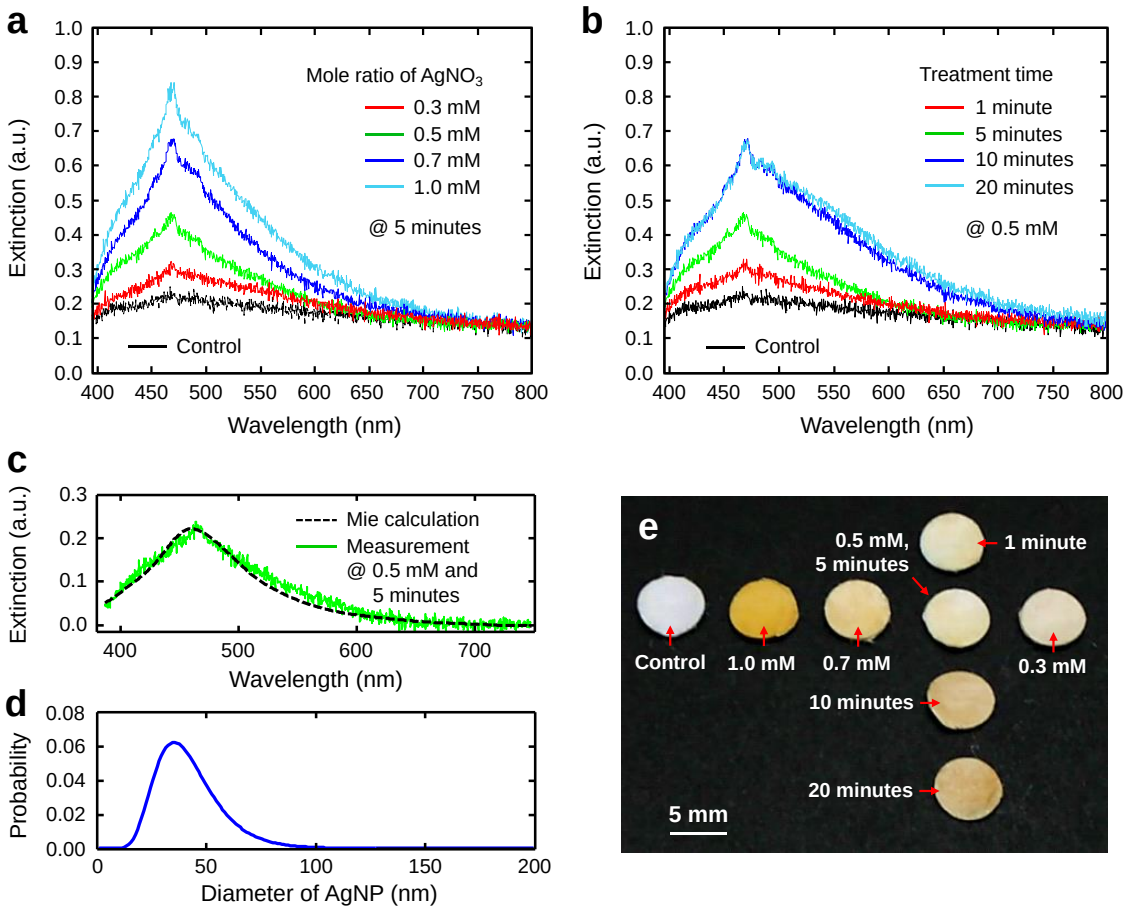

Fig. 2: Spectroscopic characterizations of AgNP-embedded in silk. (a&b) Measured extinction spectra of AgNP-embedded silk synthesized by different mole ratios of $AgNO_3$ or different treatment (dipping) times, which allow us to control the size and density of AgNPs inside silk fibers. (c) Calculated extinction spectrum using Mie theory, compared with a measured spectrum at the optimal AgNP density for photoluminescence. (d) Estimated size distribution (i.e. lognormal distribution) of AgNPs inside silk fibers by Mie theory. (e) Photograph of systematically synthesized AgNP-embedded silk specimens.

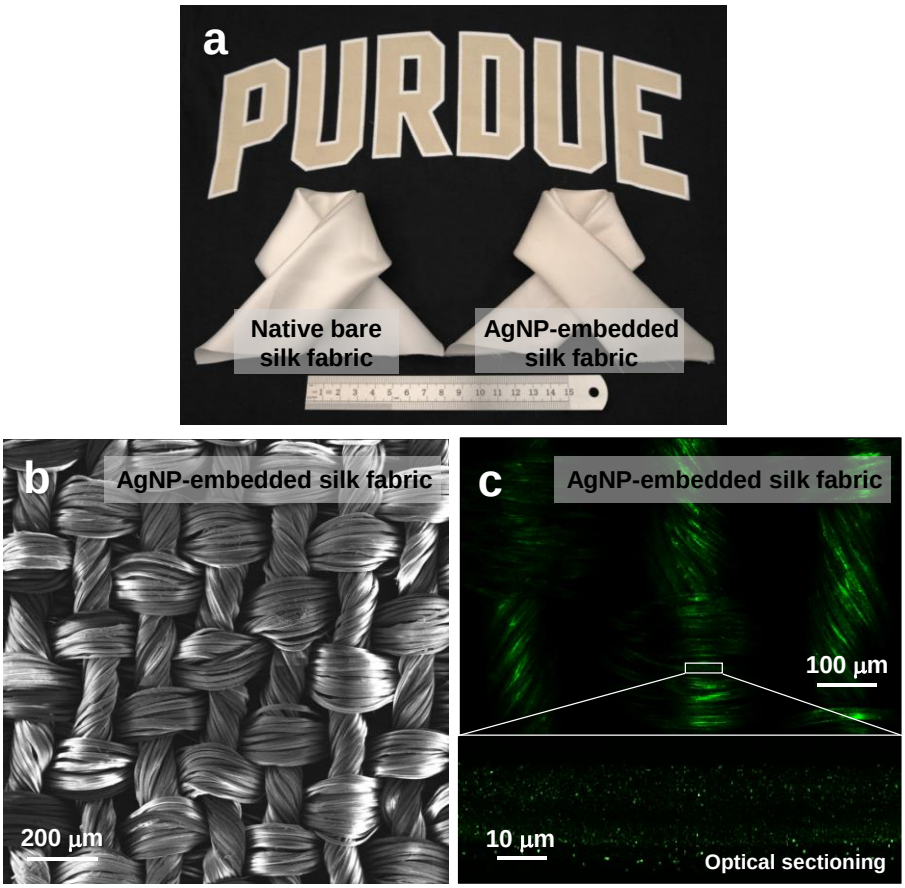

Fig. 3: Scalable and continuous nanomanufacturing using conventional textile infrastructures. (a) Photograph of native bare (control) and AgNP-embedded silk fabrics at an aqueous solution of 0.5-mM $AgNO_3$ for five minutes. (b) SEM and (c) RCM images of AgNP-embedded silk fabrics. The silk fabrics were woven without any additional chemical treatments in the Korea Silk Research Institute, Jinju, South Korea.

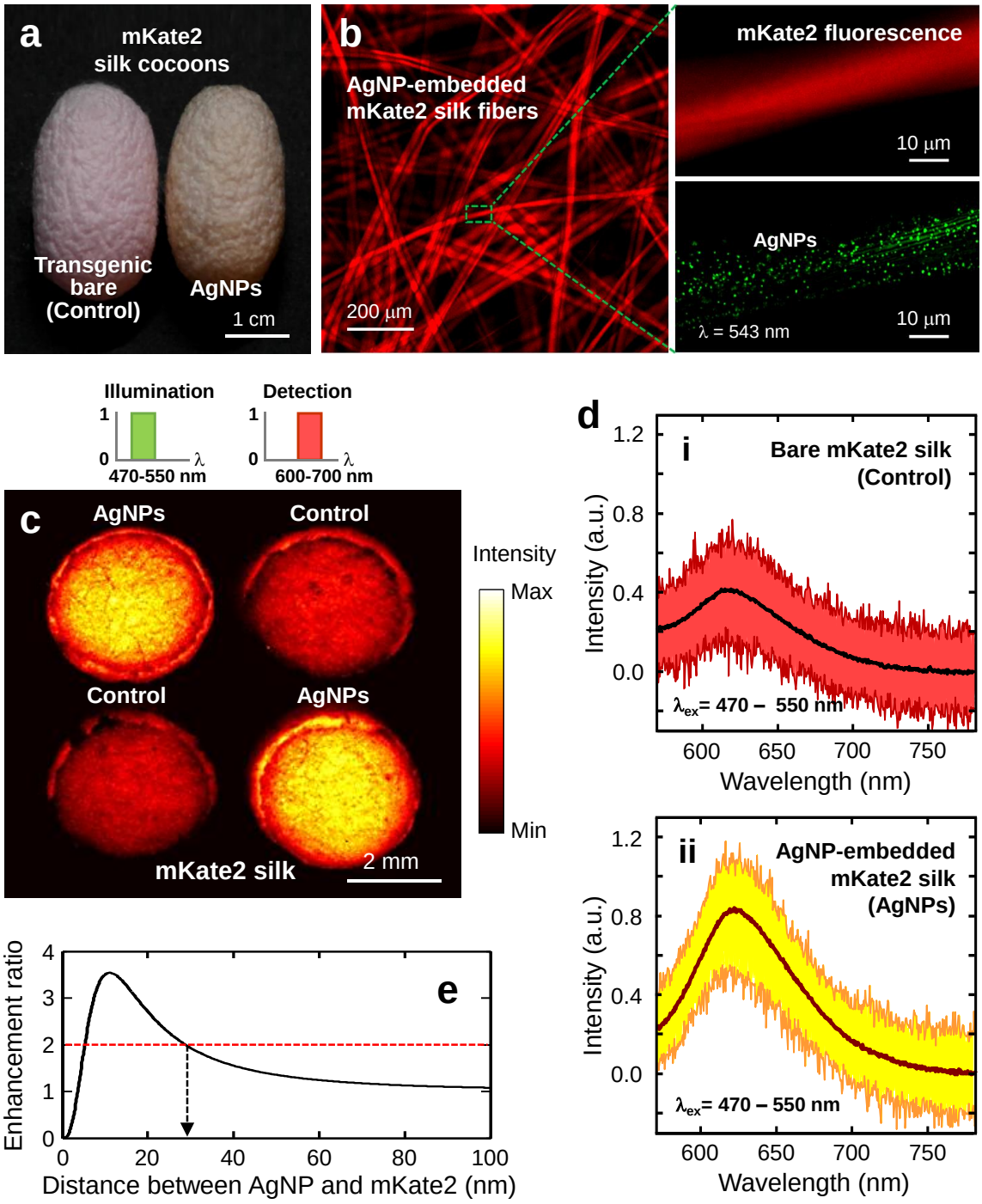

Fig. 4: Plasmon-enhanced photoluminescence of transgenic fluorescent (mKate2) silk hybridized with AgNPs. (a) Photograph of a native control mkate2 silk cocoon and an AgNP-embedded mkate2 silk cocoon synthesized under a condition of 0.5-mM $AgNO_3$ and five minutes. (b) Fluorescence confocal microscopy image of AgNP-embedded mKate2 silk fibers. Fluorescence confocal microscopy and RCM images from the same optical section of an AgNP-embedded mKate2 silk fiber, showing colocalization of mKate2 and AgNPs. (c) Fluorescent image of bare mKate2 silk (control) and AgNP-embedded mKate2 silk (AgNPs). Four different

punched specimens are arranged within the field of view of the mesoscopic imaging setup, which has excitation and emission filters as illustrated on top. (d) Emission spectra of mKate2 silk without (i) and with (ii) AgNPs under excitation λ_{ex} = 470 – 550 nm. The solid lines indicate mean values averaged from multiple fluorescent spectra, corresponding to the mKate2 silk specimens in (c). (e) Theoretical fluorescence enhancement ratio of mKate2 by AgNPs as a function of separation distance between mKate2 and AgNP. The enhancement ratio of approximately 2 (i.e. dotted red line) indicates that a possible average separation distance between mKate2 and AgNP is ~ 30 nm.

Reference

1 Coyle, S., Lau, K. T., Moyna, N., O'Gorman, D., Diamond, D., Di Francesco, F., Costanzo, D., Salvo, P., Trivella, M. G., De Rossi, D. E., Taccini, N., Paradiso, R., Porchet, J. A., Ridolfi, A., Luprano, J., Chuzel, C., Lanier, T., Revol-Cavalier, F., Schoumacker, S., Mourier, V., Chartier, I., Convert, R., De-Moncuit, H. & Bini, C. Biotex-biosensing textiles for personalised healthcare management. *Ieee Transactions on Information Technology in Biomedicine* **14**, 364-370, (2010).

2 Yetisen, A. K., Qu, H., Manbachi, A., Butt, H., Dokmeci, M. R., Hinestroza, J. P., Skorobogatiy, M., Khademhosseini, A. & Yun, S. H. Nanotechnology in textiles. *Acs Nano* **10**, 3042-3068, (2016).

3 Sengul, H., Theis, T. L. & Ghosh, S. Toward sustainable nanoproducts: An overview of nanomanufacturing methods. *Journal of Industrial Ecology* **12**, 329-359, (2008).

4 Sturzenbaum, S. R., Hockner, M., Panneerselvam, A., Levitt, J., Bouillard, J. S., Taniguchi, S., Dailey, L. A., Khanbeigi, R. A., Rosca, E. V., Thanou, M., Suhling, K., Zayats, A. V. & Green, M. Biosynthesis of luminescent quantum dots in an earthworm. *Nature Nanotechnology* **8**, 57-60, (2013).

5 Tamura, T., Thibert, C., Royer, C., Kanda, T., Abraham, E., Kamba, M., Komoto, N., Thomas, J. L., Mauchamp, B., Chavancy, G., Shirk, P., Fraser, M., Prudhomme, J. C. & Couble, P. Germline transformation of the silkworm bombyx mori l. Using a piggybac transposon-derived vector. *Nature Biotechnology* **18**, 81-84, (2000).

6 Teule, F., Miao, Y. G., Sohn, B. H., Kim, Y. S., Hull, J. J., Fraser, M. J., Lewis, R. V. & Jarvis, D. L. Silkworms transformed with chimeric silkworm/spider silk genes spin composite silk fibers with improved mechanical properties. *Proceedings of the National Academy of Sciences of the United States of America* **109**, 923-928, (2012).

7 Tansil, N. C., Koh, L. D. & Han, M. Y. Functional silk: Colored and luminescent. *Advanced Materials* **24**, 1388-1397, (2012).

8 Iizuka, T., Sezutsu, H., Tatematsu, K., Kobayashi, I., Yonemura, N., Uchino, K., Nakajima, K., Kojima, K., Takabayashi, C., Machii, H., Yamada, K., Kurihara, H., Asakura, T., Nakazawa, Y., Miyawaki, A., Karasawa, S., Kobayashi, H., Yamaguchi, J., Kuwabara, N., Nakamura, T., Yoshii, K. & Tamura, T. Colored fluorescent silk made by transgenic silkworms. *Advanced Functional Materials* **23**, 5232-5239, (2013).

9 Cai, L. Y., Shao, H. L., Hu, X. C. & Zhang, Y. P. Reinforced and ultraviolet resistant silks from silkworms fed with titanium dioxide nanoparticles. *Acs Sustainable Chemistry & Engineering* **3**, 2551-2557, (2015).

10 Kim, D. W., Lee, O. J., Kim, S. W., Ki, C. S., Chao, J. R., Yoo, H., Yoon, S. I., Lee, J. E., Park, Y. R., Kweon, H., Lee, K. G., Kaplan, D. L. & Park, C. H. Novel fabrication of fluorescent silk utilized in biotechnological and medical applications. *Biomaterials* **70**, 48-56, (2015).

11 Wang, Q., Wang, C., Zhang, M., Jian, M. & Zhang, Y. Feeding single-walled carbon nanotubes or graphene to silkworms for reinforced silk fibers. *Nano Letters* **16**, 6695-6700, (2016).

12 Hardy, J. G., Romer, L. M. & Scheibel, T. R. Polymeric materials based on silk proteins. *Polymer* **49**, 4309-4327, (2008).

13 Brenckle, M. A., Tao, H., Kim, S., Paquette, M., Kaplan, D. L. & Omenetto, F. G. Protein-protein nanoimprinting of silk fibroin films. *Advanced Materials* **25**, 2409-2414, (2013).

14 Tao, H., Kainerstorfer, J. M., Siebert, S. M., Pritchard, E. M., Sassaroli, A., Panilaitis, B. J. B., Brenckle, M. A., Amsden, J. J., Levitt, J., Fantini, S., Kaplan, D. L. & Omenetto, F. G. Implantable, multifunctional, bioresorbable optics. *Proceedings of the National Academy of Sciences of the United States of America* **109**, 19584-19589, (2012).
15 Vollrath, F. & Knight, D. P. Liquid crystalline spinning of spider silk. *Nature* **410**, 541-548, (2001).
16 Jin, H. J. & Kaplan, D. L. Mechanism of silk processing in insects and spiders. *Nature* **424**, 1057-1061, (2003).
17 Fu, C. J., Shao, Z. Z. & Fritz, V. Animal silks: Their structures, properties and artificial production. *Chemical Communications*, 6515-6529, (2009).
18 Phipson, T. L. Weighted silk. *Chamber's Journal* **1**, 44-45, (1898).
19 Chittick, J. *Silk manufacturing and its problems*. (1913).
20 Thiel, B. L. & Viney, C. Spider major ampullate silk (drag line): Smart composite processing based on imperfect crystals. *Journal of Microscopy-Oxford* **185**, 179-187, (1997).
21 Dong, Q., Su, H. L. & Zhang, D. In situ depositing silver nanoclusters on silk fibroin fibers supports by a novel biotemplate redox technique at room temperature. *Journal of Physical Chemistry B* **109**, 17429-17434, (2005).
22 Fei, X., Jia, M. H., Du, X., Yang, Y. H., Zhang, R., Shao, Z. Z., Zhao, X. & Chen, X. Green synthesis of silk fibroin-silver nanoparticle composites with effective antibacterial and biofilm-disrupting properties. *Biomacromolecules* **14**, 4483-4488, (2013).
23 Mayes, E. L., Vollrath, F. & Mann, S. Fabrication of magnetic spider silk and other silk-fiber composites using inorganic nanoparticles. *Advanced Materials* **10**, 801–805, (1998).
24 Arai, T., Freddi, G., Colonna, G. M., Scotti, E., Boschi, A., Murakami, R. & Tsukada, M. Absorption of metal cations by modified b-mori silk and preparation of fabrics with an antimicrobial activity. *Journal of Applied Polymer Science* **80**, 297-303, (2001).
25 Tsukada, M., Arai, T., Colonna, G. M., Boschi, A. & Freddi, G. Preparation of metal-containing protein fibers and their antimicrobial properties. *Journal of Applied Polymer Science* **89**, 638-644, (2003).
26 Lee, S. M., Pippel, E., Gosele, U., Dresbach, C., Qin, Y., Chandran, C. V., Brauniger, T., Hause, G. & Knez, M. Greatly increased toughness of infiltrated spider silk. *Science* **324**, 488-492, (2009).
27 Dickerson, M. B., Lyon, W., Gruner, W. E., Mirau, P. A., Slocik, J. M. & Naik, R. R. Sporicidal/bactericidal textiles via the chlorination of silk. *Acs Applied Materials & Interfaces* **4**, 1724-1732, (2012).
28 Cohen-Karni, T., Jeong, K. J., Tsui, J. H., Reznor, G., Mustata, M., Wanunu, M., Graham, A., Marks, C., Bell, D. C., Langer, R. & Kohane, D. S. Nanocomposite gold-silk nanofibers. *Nano Letters* **12**, 5403-5406, (2012).
29 Tang, B., Li, J. L., Hou, X. L., Afrin, T., Sun, L. & Wang, X. G. Colorful and antibacterial silk fiber from anisotropic silver nanoparticles. *Industrial & Engineering Chemistry Research* **52**, 4556-4563, (2013).
30 Wu, M. C., Ma, B. H., Pan, T. Z., Chen, S. S. & Sun, J. Q. Silver-nanoparticle-colored cotton fabrics with tunable colors and durable antibacterial and self-healing superhydrophobic properties. *Advanced Functional Materials* **26**, 569-576, (2016).

31 Xiu, Z. M., Zhang, Q. B., Puppala, H. L., Colvin, V. L. & Alvarez, P. J. J. Negligible particle-specific antibacterial activity of silver nanoparticles. *Nano Letters* **12**, 4271-4275, (2012).
32 Frische, Maunsbach & Vollrath. Elongate cavities and skin–core structure in nephila spider silk observed by electron microscopy. *Journal of Microscopy-Oxford* **189**, 64–70, (1998).
33 Hakimi, O., Knight, D. P., Knight, M. M., Grahn, M. F. & Vadgama, P. Ultrastructure of insect and spider cocoon silks. *Biomacromolecules* **7**, 2901-2908, (2006).
34 Du, N., Yang, Z., Liu, X. Y., Li, Y. & Xu, H. Y. Structural origin of the strain-hardening of spider silk. *Advanced Functional Materials* **21**, 772-778, (2011).
35 Giesa, T., Arslan, M., Pugno, N. M. & Buehler, M. J. Nanoconfinement of spider silk fibrils begets superior strength, extensibility, and toughness. *Nano Letters* **11**, 5038-5046, (2011).
36 Sivaraman, S. K., Elango, I., Kumar, S. & Santhanam, V. A green protocol for room temperature synthesis of silver nanoparticles in seconds. *Current Science* **97**, 1055-1059, (2009).
37 Yi, Z., Li, X. B., Xu, X. B., Luo, B. C., Luo, J. S., Wu, W. D., Yi, Y. G. & Tang, Y. J. Green, effective chemical route for the synthesis of silver nanoplates in tannic acid aqueous solution. *Colloids and Surfaces a-Physicochemical and Engineering Aspects* **392**, 131-136, (2011).
38 Beck, C. S. & Powers, J. H. Burns treated by tannic acid. *Annals of Surgery* **84**, 19-36, (1926).
39 Beekman, F. Tannic acid treatment of burns - end-results in one hundred and fourteen cases compared with three hundred and twenty treated by other methods. *Archives of Surgery* **18**, 803-806, (1929).
40 Teli, M. D. in *Advances in silk science and technology* (ed A. Basu) Ch. 5, (Elsevier, 2015).
41 Jain, P. K., Lee, K. S., El-Sayed, I. H. & El-Sayed, M. A. Calculated absorption and scattering properties of gold nanoparticles of different size, shape, and composition: Applications in biological imaging and biomedicine. *Journal of Physical Chemistry B* **110**, 7238-7248, (2006).
42 van de Hulst, H. C. *Light scattering by small particles*. (Dover Publications, 1995).
43 Kim, Y. L., Liu, Y., Wali, R. K., Roy, H. K., Goldberg, M. J., Kromin, A. K., Chen, K. & Backman, V. Simultaneous measurement of angular and spectral properties of light scattering for characterization of tissue microarchitecture and its alteration in early precancer. *Ieee Journal of Selected Topics in Quantum Electronics* **9**, 243-256, (2003).
44 Rakic, A. D., Djurisic, A. B., Elazar, J. M. & Majewski, M. L. Optical properties of metallic films for vertical-cavity optoelectronic devices. *Applied Optics* **37**, 5271-5283, (1998).
45 Parker, S. T., Domachuk, P., Amsden, J., Bressner, J., Lewis, J. A., Kaplan, D. L. & Omenetto, F. G. Biocompatible silk printed optical waveguides. *Advanced Materials* **21**, 2411-2415, (2009).
46 Kiss, L. B., Soderlund, J., Niklasson, G. A. & Granqvist, C. G. New approach to the origin of lognormal size distributions of nanoparticles. *Nanotechnology* **10**, 25-28, (1999).

47 Anger, P., Bharadwaj, P. & Novotny, L. Enhancement and quenching of single-molecule fluorescence. *Physical Review Letters* **96**, 113002, (2006).
48 Bharadwaj, P. & Novotny, L. Spectral dependence of single molecule fluorescence enhancement. *Optics Express* **15**, 14266-14274, (2007).
49 Geddes, C. D., Zhang, Y. & Dragan, A. Wavelength dependence of metal-enhanced fluorescence. *Journal of Physical Chemistry C* **113**, 12095-12100, (2009).
50 Choi, S. H., Kwak, B., Han, B. & Kim, Y. L. Competition between excitation and emission enhancements of quantum dots on disordered plasmonic nanostructures. *Optics Express* **20**, 16785-16793, (2012).
51 Wang, Z., Meng, X., Choi, S. H., Knitter, S., Kim, Y. L., Cao, H., Shalaev, V. M. & Boltasseva, A. Controlling random lasing with three-dimensional plasmonic nanorod metamaterials. *Nano Letters* **16**, 2471-2477, (2016).
52 Linic, S., Christopher, P. & Ingram, D. B. Plasmonic-metal nanostructures for efficient conversion of solar to chemical energy. *Nature Materials* **10**, 911-921, (2011).
53 Ma, X. C., Dai, Y., Yu, L. & Huang, B. B. Energy transfer in plasmonic photocatalytic composites. *Light: Science & Applications* **5**, e16017, (2016).
54 Bogdanov, A. M., Mishin, A. S., Yampolsky, I. V., Belousov, V. V., Chudakov, D. M., Subach, F. V., Verkhusha, V. V., Lukyanov, S. & Lukyanov, K. A. Green fluorescent proteins are light-induced electron donors. *Nature Chemistry Biology* **5**, 459-461, (2009).
55 Acharya, A., Bogdanov, A. M., Grigorenko, B. L., Bravaya, K. B., Nemukhin, A. V., Lukyanov, K. A. & Krylov, A. I. Photoinduced chemistry in fluorescent proteins: Curse or blessing? *Chemical Reviews* **117**, 758-795, (2017).

Chapter 2: Cooperative self-cooling of native silk

Abstract

Since radiative cooling was proposed as early as in 1970s,[1-3] this idea has recently regained considerable attention thanks to the advances in plasmonics and nanophotonics.[4-6] Although nanoscale fabrication and synthesis have shown the possibilities of thermal photonic nanomaterials and nanostructures, these are intrinsically limited for large-scale, sustainable, economical, and environmentally-friendly production. In search of biogenic nanomaterials and structures for radiative self-cooling, native silk, produced by *Bombyx mori*, appears to be an ideal candidate as possessing two distinct optical and thermal mechanisms: i) The brilliant whiteness of silk, resulting from strong light scattering, enhances reflectivity of sunlight in the visible and NIR ranges. ii) The protein and amino acid structures of native silk give rise to strong emissivity (or absorption) in the infrared (IR) region where solar radiation is negligible and thermal radiation is dominant. We report the spectral properties of silk support these combined photo-thermal mechanisms. By conducting thermal experiments, we directly verify that temperature is controlled in native silk under excessive sunlight. These results provide a better understanding of dissipating heat back to the surroundings via blackbody radiation in nature. We further envision that biogenic self-cooling of silk could potentially be a building block for large-area flexible thermal-photonics and for a scalable hybridization platform of multifunctional nanomaterials in a variety of defense applications.

Introduction

It is well known that a silk cocoon shell has multiple vital functions as a habitat of a silkworm for regulating physical and biological conditions (e.g. carbon dioxide, temperature, humidity, mechanical attack, and electrical properties).[7-10] It would also be critical for the silkworm to have a protection mechanism against heat retention from excessive sunlight, because the pupa spends the most of time inside the silk cocoon during the life cycle. Thus, one can speculate that the silk cocoon shell could potentially have a photo-thermoregulatory function, in particular for radiation heat transfer. In this respect, the optical and thermal properties of native silk may provide a clue for passive radiative cooling in nature.

Native silk possesses a distinct photonic property. The natural color of silk cocoon shells is described by the 'lustrous' or 'silvery' reflection, indicating strong light scattering and Anderson light localization in silk. In particular, strong light localization often results in the suppression of light transmission. Thus, this optical property can make silk highly reflective to solar radiation that dominates the visible and NIR region. In Fig. 5a, integrating sphere measurements show that a white cocoon shell reflects 80% of sunlight in the visible and NIR region; the reflectance values reaches 90% at 550 nm where the sunlight is strongest. In other words, as shown in the visual appearance of the brilliant whiteness, native silk effectively reflects out solar radiation.

Native silk also possesses a unique thermal radiation property. The protein and amino acid structures of native silk give rise to the strong absorption (i.e. high emissivity by Kirchhoff's identity) in IR. For the broad spectral area of first and second atmospheric transparency windows (i.e. 7 – 14 μm and 16 – 25 μm), native silk shows an extremely high thermal emissivity, which is comparable to the blackbody in Fig. 5a. Silk proteins are mainly composed with fibroin (e.g. heavy and light chains of polypeptides) and sericin.[11,12] In particular, fibroin is

composed of highly repetitive glycine and alanine-rich regions. The numerous strong absorption peaks in IR originate from molecular vibrational and rotational modes supported in the complex protein structures of silk. Predominantly, silk forms antiparallel β-sheet nanocrystals, which are mainly responsible for the mechanical properties,[13-15] determines the major absorption bands of several amides.[16] Thus, this high emissivity characteristic of native silk can be advantageous over typical synthetic cooling materials, in which the emissivity engineering of synthetic radiative coolers often rely on a single absorption peak of silicon dioxide (SiO_2) or hafnium dioxide (HfO_2) in IR.[4,17]

Results and Discussion

To experimentally validate radiative cooling of native silk, we utilize measurement testbeds for radiation heat transfer, minimizing convection and conduction heat exchange between the ambient air and native silk (and other reference materials). In the testbed, a 200-mm-diameter native silk cocoon panel, in which circular patches (diameter = 10 mm) are constructed in a fish scale pattern, is cemented with a resistance temperature detector on the surface of a polystyrene base, and is covered by a transparent acrylic box. The top of the testbed is shielded by a thin low-density polyethylene film (thickness = 19 μm), which is transparent in the entire visible-NIR-IR regions. As a conventional rooftop material, an aluminum panel is also compared, because aluminum can serve a sunlight reflector as strong as native white silk in the visible and NIR region (Fig. 5). Fig. 5b shows that the steady-state temperature of the native silk panel under direct sunlight is 10 °C below the temperature of aluminum under the solar irradiance exceeding 1,000 Wm^{-2}. In the absence of sunlight at night, a slight temperature increase (~ 0.8 ºC) in the aluminum panel agrees with the low emissivity of aluminum (Fig. 5c), compared with the night temperature of the silk and black paint-coated panels.

The backyard measurements are further investigated using a 3D multiphysics model of heat transfer, including surface-to-surface radiation, in which the unique spectral behavior of the testing materials is incorporated in the entire visible-NIR-IR regions. In Fig. 5b&c, the temperature profiles of the theoretical models are in excellent agreement with the experimental results obtained during daytime and nighttime with clear sky in late summer. This result provides an example that Anderson light localization in silk offers an integrated property of a sunlight reflector and a thermal emitter, which is often challenging to achieve using conventional reflectors or synthetic radiative coolers.

Conclusion

We envision that our results will open up largely unexplored opportunities for self-cooling effects found in nature. As one of the protection mechanisms, the silk cocoon shell provides a photo-thermoregulatory function. Our results explain that the silk cocoon itself suppresses most of transmission by strongly light localization (or strong light scattering), making silk highly reflective for solar radiation in the visible range. Also, the protein and amino acid structures of native silk intrinsically support the numerous molecular vibrational and rotational modes, making silk highly emissive for thermal radiation in the IR range. Thus, the spectral properties of native silk are ideal for the self-cooling effect, supporting the combined photo-thermal mechanisms. Indeed, native silk is a biophotonic cooler. Based on the biocompatibility and bioresorbability of silk, we further anticipate that this novel functionality can be combined with biosensing platforms for prolonged monitoring of physiological and biological changes.

Acknowledgments
This work was supported by South Korea and Asian Office of Aerospace Research and Development (FA2386-16-1-4114) from Air Force Office of Scientific Research, USA. We thank Zahyun Ku and Augustine Urbas at AFRL/RX for the guidance and assistance of thermal experiments.

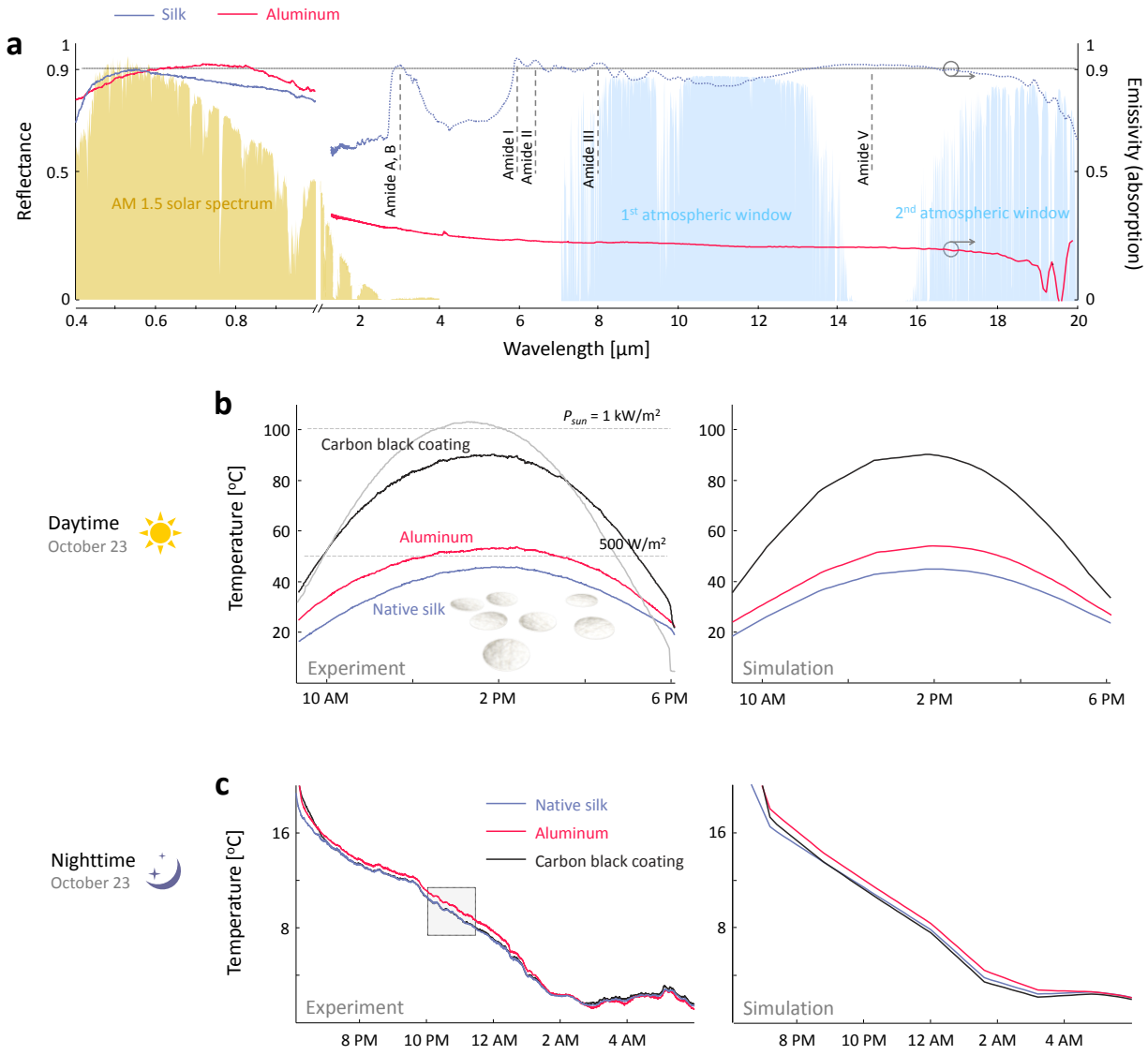

Fig. 5: Anderson light localization mediates a self-cooling function. (a) Measured reflectance and emissivity of a 400-μm-thick white silk sample from 400 nm to 20 μm (blue line). In the visible/NIR range, the entire hemispherical measurements are conducted. For the IR range, after the loss for limited NA of FTIR microscopy measurements (blue line) is compensated, the emissivity is calculated in a silk specimen with a thickness of ~100 μm. (b) Backyard measurements (left) and simulations (right) of the native silk cooling testbed (blue line), compared to other reference roofing materials (i.e. carbon black paint and aluminum). The black paint reaches a temperature up to 90 °C under direct solar irradiance power of 1,000 W/m^2 (gray line) during clear daytime of late summer. The geographic location of the backyard measurements is West Lafayette, Indiana. With an accuracy of 0.15 °C, the resistance temperature sensors monitor the back-surface temperature of each cooling panel. The temperature profiles are also simulated using a 3D multiphysics model of heat transfer. (c) Night-time radiative cooling measurements (left) and simulations (right). The measurements are conducted after 6 PM in local time during the Sun set. Night-time radiative cooling demonstration is particularly important, capturing the thermal emissivity of materials.

Reference

1 Catalanotti, S., Cuomo, V., Piro, G., Ruggi, D., Silvestrini, V. & Troise, G. Radiative cooling of selective surfaces. *Solar Energy* **17**, 83-89, (1975).

2 Harrison, A. W. & Walton, M. R. Radiative cooling of tio2 white paint. *Solar Energy* **20**, 185-188, (1978).

3 Michell, D. & Biggs, K. L. Radiation cooling of buildings at night. *Applied Energy* **5**, 263-275, (1979).

4 Raman, A. P., Anoma, M. A., Zhu, L., Rephaeli, E. & Fan, S. Passive radiative cooling below ambient air temperature under direct sunlight. *Nature* **515**, 540-544, (2014).

5 Zhu, L. X., Raman, A. P. & Fan, S. H. Radiative cooling of solar absorbers using a visibly transparent photonic crystal thermal blackbody. *Proceedings of the National Academy of Sciences of the United States of America* **112**, 12282-12287, (2015).

6 Shi, N. N., Tsai, C. C., Camino, F., Bernard, G. D., Yu, N. F. & Wehner, R. Keeping cool: Enhanced optical reflection and radiative heat dissipation in saharan silver ants. *Science* **349**, 298-301, (2015).

7 Roy, M., Meena, S. K., Kusurkar, T. S., Singh, S. K., Sethy, N. K., Bhargava, K., Sarkar, S. & Das, M. Carbondioxide gating in silk cocoon. *Biointerphases* **7**, 45, (2012).

8 Zhang, J., Rajkhowa, R., Li, J. L., Liu, X. Y. & Wang, X. G. Silkworm cocoon as natural material and structure for thermal insulation. *Materials & Design* **49**, 842-849, (2013).

9 Chen, F. J., Hesselberg, T., Porter, D. & Vollrath, F. The impact behaviour of silk cocoons. *Journal of Experimental Biology* **216**, 2648-2657, (2013).

10 Tulachan, B., Meena, S. K., Rai, R. K., Mallick, C., Kusurkar, T. S., Teotia, A. K., Sethy, N. K., Bhargava, K., Bhattacharya, S., Kumar, A., Sharma, R. K., Sinha, N., Singh, S. K. & Das, M. Electricity from the silk cocoon membrane. *Scientific Reports* **4**, 5434, (2014).

11 Hardy, J. G., Romer, L. M. & Scheibel, T. R. Polymeric materials based on silk proteins. *Polymer* **49**, 4309-4327, (2008).

12 Omenetto, F. G. & Kaplan, D. L. New opportunities for an ancient material. *Science* **329**, 528-531, (2010).

13 Vollrath, F. & Knight, D. P. Liquid crystalline spinning of spider silk. *Nature* **410**, 541-548, (2001).

14 Keten, S., Xu, Z., Ihle, B. & Buehler, M. J. Nanoconfinement controls stiffness, strength and mechanical toughness of beta-sheet crystals in silk. *Nature Materials* **9**, 359-367, (2010).

15 Perrone, G. S., Leisk, G. G., Lo, T. J., Moreau, J. E., Haas, D. S., Papenburg, B. J., Golden, E. B., Partlow, B. P., Fox, S. E., Ibrahim, A. M. S., Lin, S. J. & Kaplan, D. L. The use of silk-based devices for fracture fixation. *Nature Communications* **5**, 3385, (2014).

16 Muller, W. S., Samuelson, L. A., Fossey, S. A. & Kaplan, D. L. Formation and characterization of langmuir silk films. *Langmuir* **9**, 1857-1861, (1993).

17 Zhai, Y., Ma, Y. G., David, S. N., Zhao, D. L., Lou, R. N., Tan, G., Yang, R. G. & Yin, X. B. Scalable-manufactured randomized glass-polymer hybrid metamaterial for daytime radiative cooling. *Science* **355**, 1062-1066, (2017).